ROYAL SOCIETY
OF CHEMISTRY

PAPER

Check for updates

Sustainable agro-waste derived nitrogen-doped carbon dots for sensitive fluorescence detection of ethalfluralin residues in vegetables

Fatemeh Esfandiyari Bayat,[a] Hossein Tavallali,*[a] Mohammad Reza Baezzat[a]
and Saeed Yousefinejad ⓘ *[bc]

Ethalfluralin, a critical selective herbicide, necessitates robust and accessible detection methods to safeguard public health and ensure food safety. Current analytical techniques often suffer from complex sample preparation and high operational costs. Addressing this, we report a facile and sustainable approach for synthesizing highly photoluminescent nitrogen-doped carbon dots (N-CDs) derived entirely from agro-waste materials. This novel "green" synthesis leverages hydrothermal treatment of common vegetable biomass (lettuce, cabbage, and spinach) combined with *in situ* nitrogen doping using urea, significantly enhancing the N-CDs' optical properties. Comprehensive characterization using UV-Vis, FT-IR, fluorescence spectroscopy, XRD, TEM, and CHN analysis confirmed the successful doping and favorable physicochemical attributes of the synthesized N-CDs. Leveraging a Central Composite Design (CCD), we meticulously optimized key sensing parameters (pH, N-CDs concentration, and incubation time) to achieve maximum sensitivity. The developed N-CDs-based fluorescence sensor demonstrates exceptional analytical performance for ethalfluralin detection, exhibiting a broad linear range of 23.3–2012.9 μg kg^{-1} and a remarkably low limit of detection (LOD) of 18.8 μg kg^{-1}. Importantly, the method exhibits high applicability and provides results in good agreement with the established GC-MS technique when analyzing spiked vegetable samples, validating its accuracy and reliability. This work offers a significant advancement in eco-friendly and cost-effective pesticide residue monitoring, providing a promising alternative to conventional methods.

Sustainability spotlight

This work presents a sustainable advancement in food safety monitoring through the facile, green synthesis of highly sensitive nitrogen-doped carbon dots (N-CDs) derived entirely from agricultural waste (lettuce, cabbage, spinach). This innovative approach transforms biomass waste into valuable sensing materials, significantly reducing environmental impact and promoting resource efficiency. The developed N-CDs-based fluorescence sensor offers a cost-effective, rapid, and accurate method for detecting ethalfluralin pesticide residues in vegetables, providing a crucial eco-friendly alternative to conventional, resource-intensive techniques. This aligns strongly with UN SDG 12 (Responsible Consumption and Production) by valorizing waste and fostering sustainable material use, and SDG 2 (Zero Hunger) and SDG 3 (Good Health and Well-being) by enhancing food safety and safeguarding public health against harmful chemical contamination.

1. Introduction

Over the past decades, global environmental rules have sought to prevent diseases caused by food contaminants. The Codex Alimentarius defines a contaminant as any material not intentionally added to food, which may be present as a result of production, processing, preparation, treatment, packing,

packaging, transport, or storage, or as a result of environmental contamination.[1] Food contaminants are generally classified into three categories: physical, chemical, and biological. Chemical contaminants, which are often environmental in origin, include major groups such as mycotoxins, pesticides, veterinary drug residues, and other hazardous compounds.[2,3] Agricultural products constitute a primary source of food for the global population. However, substantial crop losses occur annually due to plant pests, leading to an increased reliance on pesticides to achieve the goal of global food for all.[4]

Despite their benefits, pesticides can have persistent, detrimental effects on both the environment and food safety. Numerous studies have demonstrated that pesticide exposure

[a]Department of Chemistry, Payame Noor University (PNU), P. O. Box 19395-4697, Tehran, Iran. E-mail: tavallali@pnu.ac.ir

[b]Research Center for Health Sciences, Institute of Health, Shiraz University of Medical Sciences, Shiraz, Iran. E-mail: yousefinejad.s@gmail.com; yousefisa@sums.ac.ir

[c]Department of Occupational Health and Safety Engineering, School of Health, Shiraz University of Medical Sciences, Shiraz, Iran

can lead to carcinogenic, teratogenic, and immunotoxic consequences in humans. Consequently, the measurement of pesticide residues has become critically important and a frequent subject of scientific investigation in recent years.[5,6]

Pesticides are broadly classified into three main categories: insecticides, herbicides, and fungicides. According to the States Environmental Protection Agency (EPA), about 40% of pesticides used during 2006–2007 belong to herbicides. Consequently, herbicides have become the predominant class of pesticides used globally for weed control in agricultural fields. Herbicides are categorized into two primary types: selective and non-selective. Selective herbicides are designed to inhibit the growth of specific weed species without harming the desired crops. In contrast, non-selective herbicides are broad-spectrum and will damage or destroy all vegetation upon contact.[6–9]

Ethalfluralin (EFA), a dinitroaniline herbicide marketed under the trade name "Sonalan," is a selective broadleaf herbicide that was first registered in 1974. Its mechanism of action involves the inhibition of root and shoot development, thereby preventing the establishment of weeds. EFA is primarily used in a variety of crops, including dry beans, sunflowers, peanuts, cucurbits, and other vegetables such as tomatoes and potatoes.[10] Human exposure to ethalfluralin (EFA) can occur through the consumption of food containing its residues. Dietary sources include plants such as cucurbits, sunflower seeds, and dry beans, as well as animal products like milk, eggs, fat, meat, and meat by-products. The European Union (EU) has set a general maximum residue limit (MRL) of 0.01 mg kg^{-1} for EFA in plants with high water and oil content. In contrast, other regulatory bodies, such as the Environmental Protection Agency (EPA), have established different MRLs; for instance, an MRL of 0.05 mg kg^{-1} is specified for crops like tomatoes.[11,12]

Various analytical techniques have been used to determine pesticide residues in food, with acceptable accuracy and precision, such as gas chromatography (GC) and liquid chromatography (LC), often coupled with mass spectrometry (MS) as a detector. Despite their reliability, these techniques present several disadvantages, including complex sample preparation requirements, the need for expensive instrumentation, and a reliance on highly skilled operators.[13] Therefore, there is a clear need for more accessible and efficient analytical techniques to determine pesticide residues. In recent decades, carbon dots (CDs), a class of fluorescent nanomaterials with a particle size typically below 10 nm, have emerged as promising sensors. Their advantages include rapid detection, low cost, low detection limits, high chemical stability, and ease of use.[14,15] Carbon dots (CDs) are typically synthesized using either "top-down" or "bottom-up" methodologies. In the top-down approach, macroscopic carbon sources, such as graphene or carbon nanotubes, are fragmented, either physically or chemically, into nanoscale carbon particles smaller than 10 nm, which predominantly feature sp^2 hybridization. In the bottom-up approach, small molecule precursors such as citric acid, urea, or ammonia are used to synthesize CDs through pyrolysis or carbonization processes. Both top-down and bottom-up methods, however, present drawbacks, including the use of toxic chemical reagents, high energy consumption, and

prolonged reaction times. To overcome these limitations, researchers have developed greener synthesis routes utilizing natural carbon sources. Among these, the hydrothermal method is a prominent technique, valued for its simplicity and ability to produce CDs with high quantum yields.[16–20] Consequently, due to its low cost and operational simplicity, the hydrothermal method has become a common technique for preparing green CDs. A key advantage of this green synthesis approach is the substitution of hazardous organic solvents, such as methanol and dimethylformamide (DMF), with water as a benign reaction medium.

The primary renewable carbon sources used in the green synthesis of CDs can be broadly categorized as human-derived materials, horticultural and agricultural products, and their associated wastes (agro-waste).[21] Natural products serve as excellent carbon sources due to their wide availability, stability, and eco-friendliness. An additional significant benefit of this approach is the valorization of waste biomass into high-value materials. In a typical hydrothermal synthesis, the renewable carbon source is placed in an autoclave reactor and heated to a temperature ranging from 120 to 350 °C for a period of 3 to 12 hours to complete the reaction.[22–24]

In the synthesis of CDs, heteroatoms are frequently employed as doping agents to enhance the fluorescence quantum yield and photoluminescence properties through surface functionalization. Consequently, significant research efforts are dedicated to developing novel doping agents and innovative doping methodologies. Among various doping agents, nitrogen is the most prevalent due to its suitable electronegativity and atomic size, a lone electron pair that can be donated into the carbon lattice of CDs, and sufficient valence electrons to form stable bonds.[25,26] In this work, lettuce, cabbage, and spinach were specifically selected as green carbon sources not only for their sustainability and high carbon content but also for their inherent nitrogen, which provides an *in situ* doping effect, and their abundance of molecular precursors such as amino acids and proteins. During the hydrothermal process, these biomolecules are readily converted into fluorescent carbon nanostructures. Furthermore, urea was employed as an auxiliary nitrogen dopant to enhance the quantum yield of the resulting CDs.[27]

In summary, this work details the development of a sensitive fluorescent sensor for ethalfluralin (EFA) herbicide, in alignment with green chemistry principles. The strategy centers on nitrogen-doped carbon dots (N-CDs), synthesized sustainably from leafy vegetable waste using urea as a dopant. The emissive properties of the N-CDs were enhanced through the incorporation of pyridinic nitrogen. Critical sensing conditions were optimized using a Central Composite Design (CCD) to maximize analytical performance. The detection mechanism is based on the inner filter effect (IFE), whereby EFA selectively quenches the fluorescence of the N-CDs under the optimized parameters. This robust approach establishes a practical and field-deployable method for monitoring EFA residues in agricultural samples.[28–30]

2 Materials and methods

2.1 Reagents and instruments

All chemicals were of analytical reagent grade and used without further purification. Ethalfluralin (EFA) standard was obtained from LGC Standards (UK). For the preparation of Britton–Robinson (BR) buffer, boric acid, phosphoric acid, acetic acid, and sodium hydroxide were procured from Merck (Germany). The Britton–Robinson (universal buffer) buffer, used for optimization, was prepared by mixing 0.04 M solutions of boric acid, phosphoric acid, and acetic acid. The pH was adjusted to the desired value (ranging from 2 to 12) using a sodium hydroxide solution (0.2 M). Urea and Rhodamine B were also procured from Merck (Germany). Rhodamine B was used as a standard to calculate the fluorescence quantum yield.

The materials employed in the QuEChERS extraction, including the salts magnesium sulfate ($MgSO_4$) and sodium chloride (NaCl), the sorbent primary secondary amine (PSA), the internal standard triphenyl phosphate, trisodium citrate, disodium hydrogen citrate 1,5 hydrate, and the solvents acetonitrile and ethyl acetate—were purchased from Sigma-Aldrich (Merck, Germany). Deionized (DI) water was produced using a Millipore Direct-Q 8 water purification system (Merck, Germany). A Metrohm 780 pH meter was used for all pH adjustments. For the lyophilization step in CDs preparation, an Alpha 1-2 LD plus freeze dryer (or Alpha 2-4 LD plus) was employed.

This study did not involve the use of any human or animal subjects. All materials used were of standard laboratory grade and were not known to be hazardous.

2.2 Preparation of nitrogen-doped carbon dots (N-CDs)

The synthesis was carried out using a hydrothermal method. Key parameters, including temperature and time, were optimized *via* the one-factor-at-a-time (OFAT) approach. Fresh agro-waste comprising lettuce, cabbage, and spinach (both leaves and stems) was sourced from a certified organic farm in Shiraz, Iran, ensuring a traceable supply and minimizing the risk of pesticide contamination. The biomass was thoroughly rinsed with deionized water, finely chopped, and homogenized in an equal mass ratio (1 : 1 : 1). For a typical synthesis, 1000 ± 1 mg of this homogenized biomass was mixed with 50 mg of urea and dispersed in 30 mL of deionized water under constant stirring. This entire methodology, from sourcing to synthesis, was centered on the use of agricultural waste and aligns with green chemistry principles by valorizing non-marketable biomass to support a circular economy and avoid competition with food resources. The mixture in a Teflon-lined stainless-steel autoclave was heated at 300 °C for 4 hours. After cooling naturally to room temperature, the resulting dark brown solution was centrifuged at 14 000 rpm for 15 minutes. The supernatant was then filtered through a 0.45 μm membrane syringe filter to remove large particles. Eventually, the synthesized N-CDs was dried by freeze dryer, diluted by water to obtain an equivalent concentration (1000 mg kg^{-1}), and stored in the refrigerator (4 °C) for further experimentations. The hydrothermal synthesis of
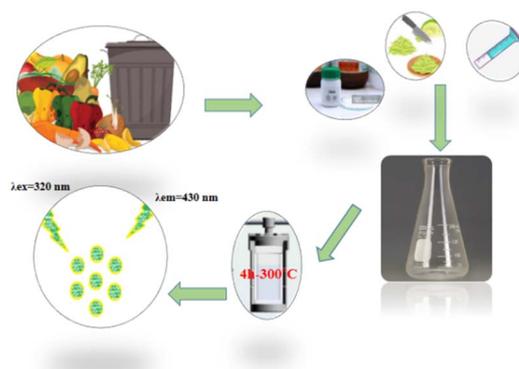

Fig. 1 Schematic illustration of the synthesis of N-CDs *via* a green method and the proposed mechanism for fluorescence-based sensing of EFA.

N-CDs from green precursors is schematically illustrated in Fig. 1.

The fluorescence quantum yields (Φ) of the synthesized non-doped CDs and nitrogen-doped carbon dots (N-CDs) were calculated using the comparative method, with Rhodamine B (Φ = 0.31 in water) employed as a reference standard. The detailed calculation procedure was provided in the SI.[31]

2.3 Characterization

The physical and chemical properties of the synthesized N-CDs were investigated using multiple techniques. The morphology, including size distribution and shape, was analyzed by transmission electron microscopy (TEM) using a LEO 906E microscope operating at an acceleration voltage of 100 kV. X-ray diffraction (XRD) analysis was performed using a Bruker D8 Advance diffractometer with Cu Kα radiation (k = 0.15418 nm) to determine the crystallographic structure of the synthesized N-CDs. Elemental analysis (CHN) was conducted using a Labtron elemental analyzer. Fourier-transform infrared (FT-IR) spectroscopy was performed on a Bruker Tensor II spectrometer equipped with a diamond iD5 ATR accessory. Spectra were recorded in the range of 4000–500 cm^{-1} to confirm nitrogen doping and identify the surface functional groups present on the N-CDs. The crystallographic nature of the synthesized N-CDs was investigated using a LabRAM HR Evolution confocal Raman microscope (Horiba) to distinguish between amorphous and graphitic structures. Furthermore, the optical properties were characterized by fluorescence spectroscopy using an LS55 spectrofluorometer (PerkinElmer, USA) and UV-Vis spectroscopy using a Shimadzu 1601 spectrophotometer.

2.4 Detection procedure of EFA by fluorescence quenching

The detection mechanism was based on the quenching of the fluorescence (FL) intensity of the N-CDs upon interaction with EFA. For the calibration curve, the net FL intensity was calculated by subtracting the intensity of the N-CDs-EFA mixture from the initial intensity of the N-CDs solution (the blank).[32] In the general detection assay, 200 μL of the N-CDs stock solution (1000 mg kg^{-1}) was mixed with 1 mL of universal buffer (pH 8.0)
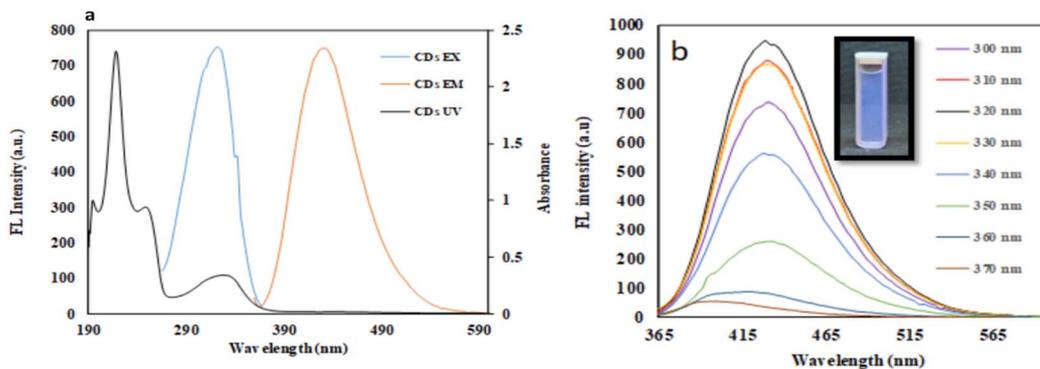
Fig. 2 Optical characteristics of the N-CDs. (a) Absorption (UV), excitation, and emission spectra. (b) Excitation-dependent emission spectra. Inset: Photograph of the N-CDs solution under 320 nm UV light.

in a quartz cuvette. Different volumes of an EFA standard solution were then spiked into the cuvette, and the mixture was diluted to a final volume of 3 mL with the same buffer. After a 5-minute incubation period (determined as optimal), fluorescence spectra were recorded with an excitation wavelength of 320 nm, and the emission was scanned from 350 to 650 nm. The maximum fluorescence emission intensity of the N-CDs was observed at 430 nm.

2.5 Real sample treatment

Tomato and cucumber samples, representing real-world commodities, were purchased from a local market (Shiraz, Iran) and sampled according to the Codex Alimentarius guidelines for sampling in pesticide residual analysis (CODEX, 1999).[33] The sampling vegetables, were subsequently washed with deionized water, air-dried at room temperature, sliced into small pieces, and homogenized. Prior to spiking, all samples

were analyzed using the GC-MS method and QuEChERS extraction to verify the absence of EFA residues, thereby establishing a reliable blank and ensuring the accuracy of subsequent quantification. To evaluate the analytical performance and potential matrix effects of the N-CDs based fluorescence sensing method, recovery studies were conducted. Vegetable samples were spiked with EFA standard at three different concentration levels: 30, 200, and 800 $\mu g\ kg^{-1}$. The spiked samples were then incubated for 24 hours to simulate potential analyte–matrix interactions and environmental stability prior to analysis. For each vegetable type, a blank (unspiked) sample was processed alongside the spiked samples. An adequate (10 ± 0.1 g) portion of each homogenized sample (spiked and blank) was combined with 10 mL of ethyl acetate and gently agitated. The mixture was then centrifuged at 5000 rpm for 15 minutes at -5 °C. The resulting organic (upper) layer was carefully collected and filtered through a 0.45 μm. The filtered extracts
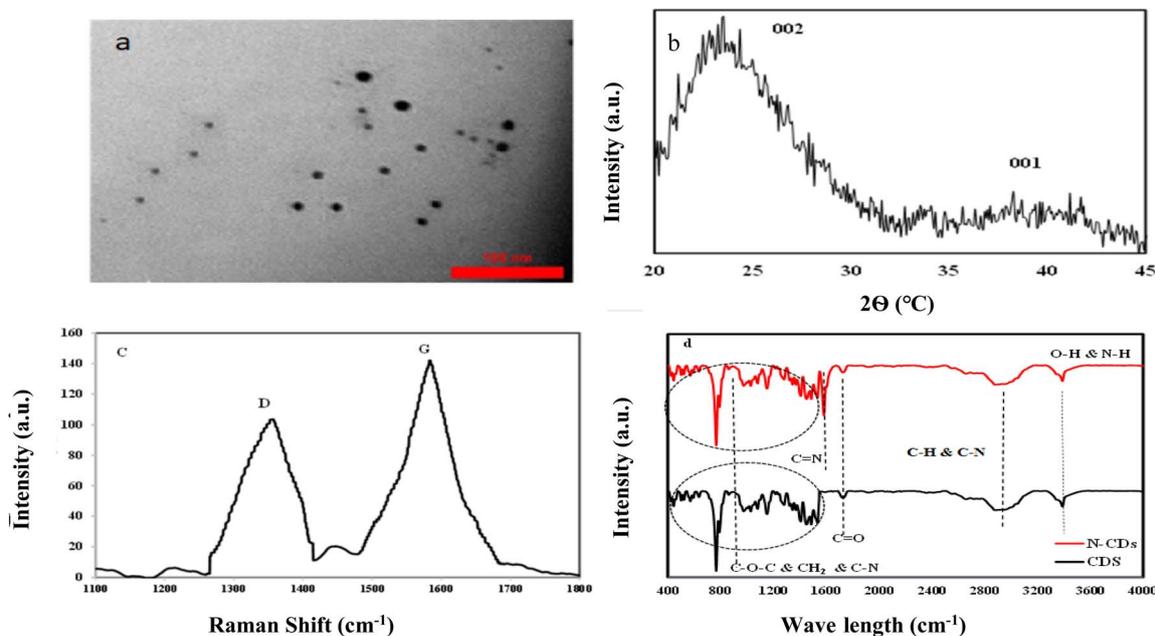

Fig. 3 Structural and chemical characterization of synthesized N-CDs. (a) TEM image. (b) XRD pattern. (c) Raman spectrum. (d) FT-IR spectrum (non-doped CDs and N-CDs).
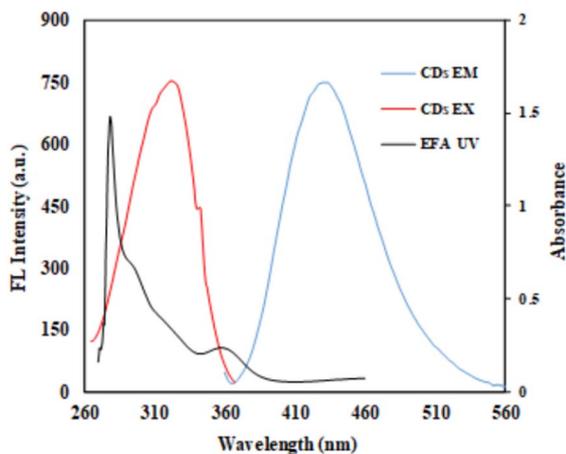
© 2026 The Author(s). Published by the Royal Society of Chemistry

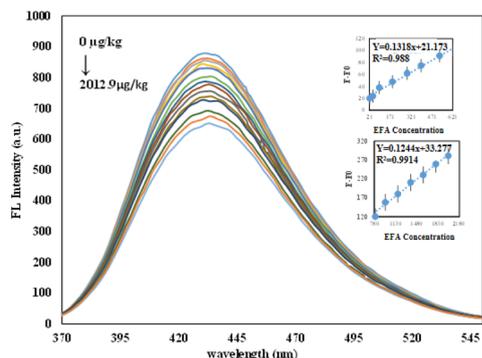**Fig. 4** Excitation and emission spectra of N-CDs alongside the absorption spectrum of EFA.

Fig. 5 Emission spectra of N-CDs with varying EFA concentrations. Inset: Calibration curves for the low (23.3–626.5 μg kg^{-1}) and high (626.5–2012 μg kg^{-1}) concentration ranges.

were analyzed using the same fluorescence sensing procedure established for standard solutions. To validate the proposed N-CDs-based method, the samples were also analyzed using gas chromatography-mass spectrometry (GC-MS) coupled with a QuEChERS extraction, performed in accordance with the standard method CEN EN 15662:2018.[30,31] Comprehensive details regarding the QuEChERS extraction procedure and the reference GC-MS method are provided in the SI.

The proposed N-CDs fluorescence sensor was statistically validated against the reference GC-MS method. An F-test was performed using Microsoft Excel 2013 to compare the variances of the two methods and evaluate the homogeneity of their precision. All statistical analyses were based on triplicate

measurements ($n = 3$) for each data point to ensure the reproducibility of the results.[20] Any replicate with a signal deviation exceeding 5% from the mean was excluded and re-measured to ensure data reliability. The analytical sensitivity was characterized by the limit of detection (LOD), calculated using eqn (1):

$$\text{LOD} = 3.3\sigma/S \qquad (1)$$

where σ is the standard deviation of the blank signal ($n = 10$) and S is the slope of the calibration curve within the linear range.

2.6 Design of experiment

Among the statistical methods used to identify and optimize significant variables, Central Composite Design (CCD) was the primary approach employed.[34] To determine the optimal sensing conditions for EFA analysis, CCD was employed. The model investigated the simultaneous effects of three significant variables: pH, N-CDs concentration, and incubation time, on the fluorescence response. Numerous studies have demonstrated that pH significantly influences the photoluminescence properties of CDs. This effect is primarily attributed to electron transfer processes induced by protonation and deprotonation of surface functional groups (*e.g.*, amine and carboxyl), which subsequently alter the fluorescence intensity. In addition to pH, other critical factors affecting CDs optical properties include their concentration, incubation time, and temperature, all of which were considered for optimization in this study.[35] The emission and excitation wavelengths for fluorescence determination, along with temperature, were optimized using the one-factor-at-a-time (OFAT) approach. The remaining critical parameters, pH, N-CDs concentration, and incubation time, were optimized simultaneously using a CCD. Initially, an appropriate range of selected factors was chosen based on the literature review.[36] Based on the three selected factors, a single-block CCD comprising 20 randomized runs was employed to minimize the effects of uncontrolled variables. The design incorporated five levels for each factor: a central point, two factorial points, and two axial points located at $-\alpha$ and $+\alpha$. The assigned values to each factor (five levels) were demonstrated in Table S1. The analysis of variance (ANOVA) was used to identify significant factors and their interaction effects. A regression model was subsequently developed to describe the relationship between these factors and the experimental response, which was defined as the change in fluorescence intensity (ΔF) for each run. All statistical design and analysis were performed using Design-Expert software (version 7.0, Stat-Ease Inc., USA).

Table 1 Two regression equations with corresponding correlation coefficients and detection limit of the proposed N-CDs fluorescence sensor^a

Linear range (μg kg^{-1})	Regression equation	Correlation coefficient	Detection limit (μg kg^{-1})
23.3–626.5	$F - F_0 = 0.132[\text{C}]^1 + 21.173$	0.988	18.8
626.5–2012.9	$F - F_0 = 0.124[\text{C}] + 33.277$	0.991	

^{a} C^1: concentration of EFA.

Table 2 Ethalfluralin (EFA) results in spiked tomatoes and cucurbits by the proposed N-CDs fluorescence sensor and reference method (GC–MS)

Sample	Spiked level ($\mu g\ kg^{-1}$)	Proposed method			Reference method (GC–MS)		
		Experimental result ($\mu g\ kg^{-1}$)	Recovery (%)	RSD	Experimental result ($\mu g\ kg^{-1}$)	Recovery (%)	RSD
Tomatoes	30	27.8 ± 0.5	92.7	3.6	29.5 ± 0.4	98.3	3.2
	200	204.0 ± 0.4	102	3.1	190.4 ± 0.4	95.2	3.1
	800	768.0 ± 0.2	96	2.6	804 ± 0.2	100.5	2.9
Cucurbits	30	28.2 ± 0.3	94	3.1	30.9 ± 0.5	103.1	3.8
	200	190.0 ± 0.2	95	2.1	211.0 ± 0.2	105.5	2.7
	800	840.1 ± 0.4	105	3.5	788.0 ± 0.5	98.5	3.1

3. Results and discussion

3.1. Characterization

3.1.1. Optical properties (spectroscopic method). The synthesized green N-CDs displayed unique fluorescence (FL) spectra with a sharp emission peak at approximately 430 nm upon excitation at a wavelength of 320 nm. UV absorption spectra analysis revealed an intense peak at 200 nm and two weaker peaks around 280 and 300 nm (Fig. 2a). The peaks at 200 and 280 nm are attributed to polyaromatic chromophores and $\pi \rightarrow \pi^*$ transitions corresponding to aromatic Sp^2 groups, respectively. As shown in Fig. 2b, an excitation wavelength of 320 nm yielded maximum emission intensity without any shift in the maximum emission wavelength. A blue illumination was observed under UV light (320 nm), as seen in the inset photograph.

The Raman spectrum (Fig. 3c) showed two distinct peaks at around 1356 and 1580 cm^{-1}, corresponding to the D and G bands, respectively. The D band is linked to sp^3 bonds, while the sharper G band indicates sp^2 bonds. An IG/ID ratio greater than 1 suggests that the structure of the synthesized N-CDs mainly consists of sp^2 carbon, with some sp^3 carbon present as defects in the synthesis process. These Raman results imply that the proposed N-CDs have a graphitic structure.

The FT-IR spectra of both non-doped and nitrogen-doped CDs (N-CDs) are shown in Fig. 3d. Both types of CDs exhibited similar characteristic peaks, including a broad band around 3390 cm^{-1} corresponding to O–H and N–H stretching vibrations. A band at 3130 cm^{-1} was attributed to C–N and C–H bending vibrations, while the peaks at 1580, 1480, and 985 cm^{-1} were associated with C–O–C, CH_2, and C–N vibrations, respectively. A key difference was observed upon comparison: the N-doped CDs showed a distinct additional peak at around 1595 cm^{-1}, which is characteristic of the C=N group. This peak was absent in the non-doped CDs. In summary, the FT-IR analysis confirms the successful nitrogen-doping of the CDs and verifies the presence of hydroxyl, carbonyl, and other hydrophilic functional groups on the surface of the synthesized green N-CDs.[37,38]

Following the comparative method described in Section 2.2, the quantum yield (Φ) of the CDS was determined to be 6% before doping and 32.5% after nitrogen doping with urea. This substantial increase demonstrates the critical role of nitrogen incorporation in enhancing the photoluminescence efficiency.

3.1.2. Structural investigation. Transmission electron microscopy (TEM) analysis revealed that the synthesized N-CDs were spherical and exhibited a uniform size distribution (Fig. 3a). The particle diameters were estimated to range from 1

Table 3 Comparison of the proposed N-CDs fluorescence sensor with literature for the determination of EFA in agricultural products

Method Sample	LOD ($\mu g\ kg^{-1}$)	LOQ ($\mu g\ kg^{-1}$)	Recovery (%)	RSD (%)	Linear range ($\mu g\ kg^{-1}$)	Ref.
Capillary GC-MS Canola seed	0.006	0.02	96	7	3–100	49
Voltammetry Cucurbit	0.36	—	98–99	1.34	0.44–44.0	55
GC-ECD-MS Soybean	—	4	94.8	5.5	—	51
GC-NCI/MS[a] Garlic	0.05	0.17	76	8	0.025–0.5	52
GC-Q-Orbitrap/MS[b] Silage	20	50	114.2	<20	0.1–50	53
GC-MS-MS Tomato	1.4	5	83.3	9.9	0.5–100	54
Proposed N-CDs Tomato and cucurbit	18.8	23.3	98.1[c]	1.3	23.3–2012.9	This work

[a] GC-NCI/MS: gas chromatography-negative chemical ionization-mass spectrometry. [b] GC-Q-Orbitrap/MS: Gas-Chromatography-Quadrupole/Orbitrap Mass Spectrometry. [c] Average values.

to 12 nm. While the spherical morphology is clear, discernible lattice fringes were not observed in the TEM images, which may be attributed to the predominantly instrumental resolution limitations. The X-ray diffraction (XRD) pattern was recorded in the 2θ range of 20° to 60° with a scanning rate of 0.07° s^{-1} (Fig. 3b). The pattern exhibited two broad diffraction peaks centered at approximately 23° and 39°, which correspond to the (002) and (100) planes of graphitic carbon, respectively. This confirms the formation of a carbon structure with graphitic domains. The particle size distribution, as shown by TEM images, was consistent with and provided a morphological explanation for the broadened peak observed in the XRD pattern.

The results of the CHN elemental analysis for both non-doped CDs and N-CDs are presented in Table S2. The data confirm the successful incorporation of nitrogen into the CDs structure during synthesis. This result is consistent with other characterizations, such as the observed increase in quantum yield following nitrogen doping.[39,40]

3.1.3. Characterization of nitrogen doping configurations. The type of nitrogen configuration incorporated into the structure related to CDs was investigated by correlating the synthetic route with optical characterization and property analysis. The hydrothermal method, employing urea as a small-molecule doping agent, is well-documented to facilitate nitrogen incorporation primarily at the edges of the developing carbon lattice, favouring the formation of pyridinic nitrogen. The spectroscopic data strongly supported this assignment.

As observed, the FT-IR spectrum of the N-CDs (Fig. 3d) showed the emergence of a distinctive signature for C=N bonds in the range of 1550–1650 cm^{-1}, which corresponds to aromatic structures containing nitrogen, which was absent in the spectrum of the non-doped CDs.[27] The functional significance of the pyridinic configuration was demonstrated by the substantial enhancement in quantum yield and the specific fluorescence quenching response to the electron-accepting EFA molecule. These optical properties are directly attributed to the lone electron pair on pyridinic nitrogen, which creates localized electron-rich sites on the CDs surface. These sites serve a dual role: as efficient radiative recombination centers that enhance fluorescence, and as high-affinity binding sites for EFA that facilitate electron transfer. Collectively, these findings confirm that nitrogen is predominantly incorporated in the pyridinic form within the N-CDs structure[41,42]

3.2. Design of experiment

3.2.1. Identification and optimization of significant factors. A factorial design was implemented to identify the most significant factors affecting the fluorescence (FL) sensing of ethalfluralin (EFA) residues. The design, comprising 20 randomized experimental runs and their corresponding fluorescence responses, is detailed in Table S3. This table provides a comprehensive overview of the factor combinations and their impact on sensing performance. The emission intensity was used as the experimental response for the subsequent analysis of variance (ANOVA), the results of which are presented in Table

S4. Initially, a full quadratic model was fitted to evaluate the significance of all factors and their interactions. Based on the statistical analysis (P-values), three main factors; pH, N-CDs concentration, and incubation time, were identified as significant. However, some of their two-factor interactions were found to be statistically insignificant ($P > 0.1$) and were consequently removed from the final model to enhance its robustness and predictability.[28] Initially, a full quadratic model was fitted to evaluate the significance of all factors and their interactions. Based on the statistical analysis (P-values), three main factors; pH, N-CDs concentration, and incubation time, were identified as significant. The model was then refined by removing statistically insignificant two-factor interactions ($P > 0.1$) to enhance the robustness and predictive power of the final model. These results demonstrated that these factors significantly impact the fluorescence (FL) sensing process.

The response surface methodology (RSM) with 5 levels ($\alpha-$, $1-$, 0, 1, $\alpha+$) was employed to find the optimal values related to significant factors. As mentioned previously, a polynomial regression model, the selected variable quadratic model (SVM), was chosen due to its superior correlation coefficients, including R^2 of prediction ($R_{Pred.}^2$), R^2 adjusted ($R_{adj.}^2$), R^2 lack of fit, and R^2 calibration ($R_{cal.}^2$) (Table S4). The final uncoded (actual variables) equation based on the selected variable quadratic model is given in eqn (2) to describe the response (fluorescence emission intensity):

$$\text{Fluorescence emission intensity} = 16.06 + 1.37 \times (\text{pH}) + 0.03 \\ \times (\text{CDs concentration}) - 0.94 \\ \times (\text{incubation time}) + 0.005 \\ \times (\text{CDs concentration} \times \text{incubation time}) \quad (2)$$

Compared to the initial full quadratic model, the final reduced model suggest a more straightforward and simplified equation, enhancing its practical utility for predicting the fluorescence response. As observed in Table S4, all variables in the SVM model exhibited a p-value lower than 0.1, except incubation time. However, this factor was retained in the model because of its involvement in the interaction between the concentration of CDs and incubation time, which played a role in the final equation. AS the full variable model (FM), the p-value associated with the Selected Variable Model (SVM) indicated that the model was significant, while the lack of fit was insignificant. By comparing the statistical results of two designed models (FM, SVM), it was identified that the F-values of the model increased from 34.6 to 62.2, while the F-value of lack of fit remained approximately constant in both models. Based on literature reviews, correlation coefficients related to the refined model ($R_{cal.}^2 = 0.94$) and $R_{adj.}^2 = 0.93$ indicate sufficient goodness of fit,[28] and also, the prediction ability of the refined model improved by an increase in $R_{pred.}^2$ (increased to 0.88).

"Adequate precision" refers to a performance measure that evaluates the signal-to-noise ratio by comparing the criteria of predicted values with the average error associated with the prediction process. In the final proposed model, "adequate

precision" increased from 20 to 27.2 when ratios greater than 4 confirmed adequate model distributions.[28,43]

Fig. S1A presents a normal probability plot *versus* internally studentized residuals, displaying a straight line with moderate deviations. This pattern indicated that the error followed a normal distribution, confirming the underlying assumption of the statistical analysis. In Fig. S1C, errors distribution (residual) *vs.* runs were illustrated. As observed, the data points were randomly distributed around the zero line within the acceptable range ($\pm 3\sigma$), with an equal number of negative and positive point obtained data.[44] Fig. S1B depicted a strong correlation between the actual fluorescence (FL) intensity responses and the predicted values, further validating the model's accuracy. The R^2 value of the model (0.94) and the $R_{adj.}^2$ value (0.93) demonstrated the high accuracy and predictive ability of the proposed model. These results suggest that the SVM model effectively represents the experimental outcomes and offers a reliable method for predicting the fluorescence sensing performance of N-CDs in detecting EFA.[45]

3.2.2. Comparison of variables interaction. Three-dimensional (3D) surface plots Fig. S2A–C were used to investigate the effect of significant interaction in the designed model. In these plots, the impact of two interactions between variables was drawn *versus* the response surface while the third variable was considered fixed at the center level of the CCD plot. As can be observed, the slope of the surface plot for the interaction of pH *versus* concentration of CDs had a low slope, and the interaction of incubation time and pH has a complex surface due to inflection in its 3D surface. The interaction between the concentrations of CDs *versus* incubation time had the sharpest slope. Interestingly, the interaction between CDs concentration and incubation time was the only interaction that remained in the final equation, and the other interactions were eliminated.

3.2.3. Optimal conditions. After identifying the significant variables, the CCD software used the simplex algorithm to find the optimized values in fluorescence sensing. The final optimized conditions for the fluorescence sensing of EFA were determined as follows: pH 8.0, an N-CDs volume of 200 μL (1000 ppm), and an incubation time of 5 minutes. The close agreement between the experimental results (fluorescence intensity) obtained under optimal conditions and the values predicted by the model further validates the accuracy and reliability of the proposed model. This agreement demonstrates the effectiveness of the model in identifying significant factors and optimizing the conditions for fluorescence (FL) sensing of EFA using N-CDs.

3.3. Interaction mechanism of EFA and N-CDs

To elucidate the sensing mechanism, the excitation and emission spectra of the N-CDs were compared with the UV-Vis absorption spectrum of EFA (Fig. 4). A significant spectral overlap was observed, suggesting that the fluorescence quenching likely occurs *via* an inner filter effect (IFE). To confirm the IFE mechanism, two validation methods were employed: (1) application of the Lakowicz correction formula for fluorescence, and (2) comparison of the experimental absorption spectrum of the N-CDs-EFA mixture with the arithmetic sum of the individual N-CDs and EFA spectra. The results from both approaches confirmed the IFE as the dominant quenching mechanism. Detailed results of this analysis are provided in the SI.[41,42]

3.4. Analytical characteristics

As described in the methodology, the assay was performed by mixing the optimum volume of N-CDs (200 μL) with varying volumes of a standard EFA solution and diluting the mixture to a final volume of 3 mL with universal buffer (pH 8.0). The solutions were vortexed thoroughly and then incubated at ambient temperature for 5 minutes before fluorescence measurement. The fluorescence emission spectra of the final solutions, recorded under 320 nm excitation, were shown in Fig. 5 for EFA concentrations ranging from 23.3 to 2012.9 μg kg^{-1}. As demonstrated, the fluorescence intensity of the N-CDs decreases progressively with increasing EFA concentration, confirming a concentration-dependent quenching effect. The inset illustrates the relationship between the change in fluorescence intensity ($F_0 - F$) and the EFA concentration at the emission maximum of 430 nm, where F_0 and F represent the fluorescence intensity in the absence and presence of EFA, respectively. As shown in the inset of Fig. 5, a linear relationship was observed across two concentration ranges: 23.3–626.5 μg kg^{-1} and 626.5–2012.9 μg kg^{-1}. The corresponding linear regression equations, correlation coefficients, and the calculated limit of detection (LOD) are summarized in Table 1.

The selectivity of the N-CDs-based sensor for EFA was evaluated against all at the same concentration (393.3 μg kg^{-1}) various competing herbicides, including trifluralin, benefin, isopropalin, pirimicarb, propiconazole, clomazone, triflumizole, fenbuconazole, tetraconazole, abamectin, dinotefuran, fluopicolide, spirodiclofen, and flubendiamid. As shown in Fig. S4, no significant fluorescence quenching was observed for these potential interferents, confirming the high selectivity of the probe for EFA in complex agricultural samples.

3.5. Analysis of real samples

The practical applicability of the proposed N-CDs sensor was evaluated by detecting EFA in real agricultural samples. The sensor's performance was compared against the standard GC-MS method with QuEChERS extraction by analyzing pesticide-free tomato and cucurbit samples spiked with known concentrations of EFA. The analytical results are summarized in Table 2. The recovery percentages for the N-CDs fluorescence method ranged from 92.7% to 105.0% with relative standard deviations (RSDs) of 2.1–3.6% ($n = 3$). The GC-MS method yielded recoveries of 95.2–105.5% with RSDs of 2.7–3.8% ($n = 3$). As observed, the recovery values for both methods are comparable, indicating that the extraction procedure is effective for EFA sensing using the proposed N-CDs-based method. Furthermore, the low and compatible RSD values demonstrate the good precision of the proposed methodology.

A one-way ANOVA (single factor) was performed using Microsoft Excel (2013) to evaluate any significant difference

between the two methods. The calculated F-values for tomato (0.00064) and cucurbit (0.00077) were significantly lower than the critical F-value (7.7). This statistical comparison demonstrates no significant difference between the proposed sensor and the reference GC-MS method, confirming that both techniques are effective for the accurate detection and quantification of EFA in complex real samples.

3.6. A comparative analysis of the proposed N-CDs fluorescence sensor with conventional methods and carbon-based nanomaterials

The optical properties of the proposed N-CDs were compared to existing N-CDs. A quantum yield of 32.5% positions these N-CDs competitively against other N-CDS derived from sustainable biomass. While the hydrothermal synthesis method aligns with works such as Issa et al.,[20,27] the initial precursor used in this study offers environmental sustainability, thereby validating the efficacy of our green synthesis protocol. Furthermore, this work demonstrates that ubiquitous, low-cost leafy vegetables can serve as effective carbon sources for fabricating highly fluorescent N-CDs without compromising performance, thereby expanding the repertoire of viable biomass precursors for specific sensing applications.[27,46–48]

From an environmental sustainability perspective, the proposed N-CDs sensor possesses greener profile than the methods listed in Table 3. Its advantages include aqueous-based operation, minimal organic solvent consumption, low energy requirements, and the use of non-toxic, sustainably sourced materials. These results collectively underscore the potential of the developed fluorescent sensor as a reliable, sensitive, and environmentally friendly alternative for monitoring EFA in agricultural products.

To the best of our knowledge, no prior study has reported the detection of EFA residues using a fluorescent sensing probe. A comparison of common analytical methods for EFA determination in plant-based foodstuffs is provided in Table 3. As shown, the proposed fluorescence sensor based on green N-CDs exhibits superior precision, as indicated by its comparatively lower relative standard deviation (RSD) values. Furthermore, the developed sensor offers a wider linear dynamic range than most other reported methods for EFA detection. The average recovery values achieved are also highly competitive with those of established techniques.[49–54]

4. Conclusion

This study successfully established a robust fluorescent sensing platform utilizing green-synthesized nitrogen-doped CDs (N-CDs) for the sensitive and selective detection of EFA. The sensor demonstrated excellent analytical performance, with a broad linear range (23.3–2012.9 μg kg^{-1}) and a low detection limit of 18.8 μg kg^{-1}. The methodology, which operates via the inner filter effect (IFE), presents a rapid and cost-effective alternative to complex instrumental techniques for EFA monitoring. While the sensor shows great promise, its adoption for regulatory applications requires further validation across

a wider range of complex, real-world matrices, with performance benchmarked against established gold-standard methods like GC-MS. Future work will focus on the rational design of novel CDs with enhanced properties to detect a broader spectrum of pesticide residues. Concurrently, integrating this sensing technology into portable, user-friendly devices will be crucial for enabling convenient, on-site analysis. These advancements hold significant potential to revolutionize environmental monitoring, improve pesticide management, and safeguard food safety and public health.

Author contributions

Fatemeh Esfandiyari Bayat: writing – review & editing, writing – original draft, visualization, investigation, formal analysis, data curation. Hossein Tavallali: writing – review & editing, funding acquisition, supervision, methodology, conceptualization. Mohammad Reza Baezzat: writing – review & editing, methodology, conceptualization. Saeed Yousefinejad: writing – review & editing, visualization, validation, supervision, resources, project administration, methodology, investigation, conceptualization, data curation.

Conflicts of interest

There are no conflicts to declare.

Data availability

Most details are available as supplementary information (SI). More information and datasets used and/or analysed during the current research available from the corresponding author on reasonable request. Supplementary information: four figures (Fig. S1–S4), four tables (Tables S1–S4), and three detailed sections titled 'Determination of quantum yield', 'QuEChERS and GC-MS method' and 'Interaction mechanism of EFA and N-CDs'. See DOI: **https://doi.org/10.1039/d5fb00466g**.

Acknowledgements

References

1 H. N. Bayaga and C. N. Mbala, *Health sci. dis.*, 2023, **24**, 12, DOI: **10.5281/hsd.v24i12Suppl1.5079**.

2 D. J. Benford, Risk assessment of chemical contaminants and residues in foods, *Persistent Organic Pollutants and Toxic Metals in Foods*, Elsevier, 2013, pp. 173–187.

3 C. Wieck and J. H. Grant, *EuroChoices*, 2021, **20**, 37–47, DOI: **10.1111/1746-692X.12293**.

4 J. V. Rohit ,V. N. Mehta ,A. B. Patel, et al., Carbon dots-based fluorescence spectrometry for pesticides sensing, *Carbon Dots in Analytical Chemistry*, Elsevier, 2023, pp. 97–108.

5   F. Ashrafi Tafreshi, Z. Fatahi, S. F. Ghasemi, *et al.*, *PLoS ONE*, 2020, **15**, e0230646, DOI: **10.1371/journal.pone.0230646**.

6   J. Fenik and M. Tankiewicz MandBiziuk, *Trends Anal. Chem.*, 2011, **30**, 814–826, DOI: **10.1016/j.trac.2011.02.008**.

7   P. Kaewsuya, W. E. Brewer, J. Wong, *et al.*, *J. Agric. Food Chem.*, 2013, **61**, 2299–2314, DOI: **10.1021/jf304648h**.

8   D. Sharma, A. Nagpal, Y. B. Pakade, *et al.*, *Talanta*, 2010, **82**, 1077–1089, DOI: **10.1016/j.talanta.2010.06.043**.

9   N. Tresnakova and J. Stara AandVelisek, *Appl. Sci.*, 2021, **11**, 9004, DOI: **10.3390/app11199004**.

10 W. Avilés-Baeza, J. H. Ramírez-Silva and M. G. Lozano-Contreras, *Sci Res*, 2023, **10**, 1–7, DOI: **10.4236/oalib.1111022**.

11 N. Donley, C. Cox, K. Bennett, *et al.*, *Environ. Health Perspect.*, 2024, **132**, 075003, DOI: **10.1289/EHP13954**.

12 N. S. Khatri KandBoyd, *Weed Technol.*, 2025, **39**, e11, DOI: **10.1017/wet.2024.98**.

13 J. Wang, X. Teng, Y. Wang, *et al.*, *TrAC Trends Anal Chem*, 2021, **144**, 116430, DOI: **10.1016/j.trac.2021.116430**.

14 N. Alvandi, S. Assariha, N. Esfandiari, *et al.*, *Nanostruct & Nanoboct*, 2021, **26**, 100706, DOI: **10.1016/j.nanoso.2021.100706**.

15 H. Tavallali, G. Deilamy-Rad, A. Parhami, *et al.*, *J. Hazard. Mater.*, 2014, **266**, 189–197, DOI: **10.1016/j.jhazmat.2013.12.026**.

16 A. A. Ensafi, S. H. Sefat, N. Kazemifard, *et al.*, *Sens. Actuators, B*, 2017, **253**, 451–460, DOI: **10.1016/j.snb.2017.06.163**.

17 N. Tejwan, S. K. Saha and J. Das, *Adv. Colloid Interface Sci.*, 2020, **275**, 102046, DOI: **10.1016/j.cis.2019.102046**.

18 W. Fawaz, J. Hasian and I. Alghoraibi, *Sci. Rep.*, 2023, **13**, 18641, DOI: **10.1038/s41598-023-46084-1**.

19 M. A. Karimi, M. A. Mozaheb, A. Hatefi-Mehrjardi, *et al.*, *Sci. Iran.*, 2015, **22**, 2736–2744.

20 M. A. Issa, H. Zentou, Z. H. Jabbar, *et al.*, *Environ. Sci. Pollut. Res.*, 2022, **29**, 86859–86872.

21 N. Rabiee and R. S. Iravani SandVarma, *Molecules*, 2022, **27**, 6186.

22 H. H. Jing, F. Bardakci, S. Akgöl, *et al.*, *J. Funct. Biomater.*, 2023, **14**, 27, DOI: **10.3390/jfb14010027**.

23 S. Chahal, J.-R. Macairan, N. Yousefi, *et al.*, *RSC Adv.*, 2021, **11**, 25354–25363, DOI: **10.1039/D1RA04718C**.

24 V. Bressi, A. M. Balu, D. Iannazzo, *et al.*, *Curr. Opin. Green Sustainable Chem.*, 2023, **40**, 100742, DOI: **10.1016/j.cogsc.2022.100742**.

25 S. Munusamy, T. R. Mandlimath, P. Swetha, *et al.*, *Environ. Res.*, 2023, **231**, 116046, DOI: **10.1016/j.envres.2023.116046**.

26 S. Miao, K. Liang, J. Zhu, *et al.*, *Nano Today*, 2020, **33**, 100879, DOI: **10.1016/j.nantod.2020.100879**.

27 M. Z. Abdullah Issa, Z. Abidin, S. Sobri, *et al.*, *Nanomaterials*, 2019, **9**, 1500.

28 G. Nikaeen, S. Yousefinejad, S. Rahmdel, *et al.*, *Sci. Rep.*, 2020, **10**, 9642, DOI: **10.1038/s41598-020-66357-3**.

29 F. Nemati, M. Hosseini, R. Zare-Dorabei, *et al.*, *Sens. Actuators, B*, 2018, **273**, 25–34, DOI: **10.1016/j.snb.2018.05.163**.

30 A. Damokhi, S. Yousefinejad, S. Jafari, *et al.*, *J. Mol. Liq.*, 2023, **386**, 122506, DOI: **10.1016/j.molliq.2023.122506**.

31 S.-L. Hu, K.-Y. Niu, J. Sun, *et al.*, *J. Mater. Chem.*, 2009, **19**, 484–488.

32 Y. Yuan, J. Jiang, S. Liu, *et al.*, *Sens. Actuators, B*, 2017, **242**, 545–553, DOI: **10.1016/j.snb.2016.11.050**.

33 T. Prapamontol, S. Hongsibsong, W. Naksen, *et al.*, *Nat. Sci.*, 2021, **20**, e2021002.

34 S. Abbaszadeh, S. Yousefinejad, S. Jafari, *et al.*, *J. Sep. Sci.*, 2021, **44**, 3126–3136, DOI: **10.1002/jssc.202100044**.

35 C. Liu, F. Zhang, J. Hu, *et al.*, *Front. Chem.*, 2021, **8**, 605028, DOI: **10.3389/fchem.2020.605028**.

36 X. Luo, W. Zhang, Y. Han, *et al.*, *Food Chem.*, 2018, **258**, 214–221, DOI: **10.1016/j.foodchem.2018.03.032**.

37 P. F. Andrade, G. Nakazato and N. Durán, Additive interaction of carbon dots extracted from soluble coffee and biogenic silver nanoparticles against bacteria, *J. Phys.: Conf. Ser.*, 2017, 838012028.

38 S. A. Mathew, P. Praveena, S. Dhanavel, *et al.*, *RSC Adv.*, 2020, **10**, 24386–24396, DOI: **10.1039/D0RA04599C**.

39 A. P. P. Zattar, G. L. Fajardo, J. P. de Mesquita, *et al.*, *Fullerenes, Nanotubes Carbon Nanostruct.*, 2021, **29**, 414–422, DOI: **10.1080/1536383X.2020.1854742**.

40 A. O. da Silva, M. O. Rodrigues, M. H. Sousa, *et al.*, *Colloids Surf., A*, 2021, **621**, 126578, DOI: **10.1016/j.colsurfa.2021.126578**.

41 H. Liu, C. Xu, Y. Bai, *et al.*, *Spectrochim. Acta, Part A*, 2017, **171**, 311–316.

42 H. Fan, G. Q. Xiang, Y. Wang, *et al.*, *Spectrochim. Acta, Part A*, 2018, **205**, 221–226.

43 N. Fazeli Burestan, A. H. Afkari Sayyah and E. Taghinezhad, *Food Sci. Nutr.:Curr. Issues Answers*, 2020, **8**, 4134–4144, DOI: **10.1002/fsn3.1703**.

44 S. Yousefinejad, F. Honarasa, F. Abbasitabar, *et al.*, *J. Solution Chem.*, 2013, **42**, 1620–1632, DOI: **10.1007/s10953-013-0062-2**.

45 S. Yousefinejad and N. Honarasa FandSaeed, *J. Sep. Sci.*, 2015, **38**, 1771–1776, DOI: **10.1002/jssc.201401427**.

46 P. M. Yahaya, A. Z. Zainal, S. Abdul Rashid, *et al.*, *Processes*, 2019, **7**, 704.

47 P. M. Yahaya, A. Z. Zainal, S. Abdul Rashid, *et al.*, *Nanomaterials*, 2020, **10**, 315.

48 A. Tiwari, S. Walia, S. Sharma, *et al.*, *J. Mater. Chem. B*, 2023, **11**, 1029–1043.

49 D. D. Shackelford, R. W. McCormick, S. D. West, *et al.*, *J. Agric. Food Chem.*, 2000, **48**, 4422–4427, DOI: **10.1021/jf000250z**.

50 T. Thriveni, J. R. Kumar, J. Y. Lee, *et al.*, *Environ Monit Assess*, 2009, **151**, 9–18, DOI: **10.1007/s10661-008-0283-9**.

51 K. G. Ahn, G. P. Kim, Y. S. Hwang, *et al.*, *Korean J. Environ. Agric.*, 2018, **37**, 104–116, DOI: **10.5338/KJEA.2018.37.2.12**.

52 G.-h. Xia, W.-j. Shen, B. Wu, *et al.*, *Chromatographia*, 2014, **77**, 493–499, DOI: **10.1007/s10337-013-2618-0**.

53 Y. Xie, X. Wu, Y. Song, *et al.*, *Agriculture*, 2022, **12**, 1231, DOI: **10.3390/agriculture12081231**.

54 O. I. Abdallah, *Chem. Pap.*, 2020, **74**, 2311–2326, DOI: **10.1007/s11696-020-01075-8**.

55 T. Thriveni, J. R. Kumar, J. Y. Lee, *et al.*, *Environ. Monit. Assess.*, 2009, **151**, 9–18, DOI: **10.1007/s10661-008-0283-9**.